

Research

Numerical Simulations of Buried Emitter Back-Junction Solar Cells

Nils-P. Harder^{1*,†}, Verena Mertens¹ and Rolf Brendel^{1,2,‡}¹Institute for Solar Energy Research Hameln GmbH (ISFH), D-31860 Emmerthal, Germany²Leibniz University Hannover, Germany

We recently introduced the buried emitter back-junction solar cell, featuring large area fractions of overlap between n^+ -type and p^+ -type regions at the rear side of the device. In this paper we analyse the performance of the buried emitter solar cell (BESC) and its generalisations by one-dimensional device simulations and analytical model calculations. A key finding is that the generalised versions of the BESC structure allows achieving very high efficiencies by passivating virtually the entire surface of p -type emitters by an oxidised n -type surface layer. A disadvantage of this type of full-area emitter passivation in the generalised back-junction BESC is the need for an insulating layer between the metallisation of the emitter and the contact to the base, which is technologically difficult to achieve. Copyright © 2009 John Wiley & Sons, Ltd.

KEY WORDS: energy conversion; photodiodes; photovoltaic cell doping; photovoltaic cell fabrication; photovoltaic cells; silicon; simulation

Received 16 September 2008; Revised 10 November 2008

INTRODUCTION

Back-junction solar cells are one of the most promising high-efficiency solar cell concepts for industrially relevant high-quality monocrystalline silicon wafer material such as n -type Cz silicon. This solar cell concept benefits from the absence of optical shading by front contacts as back-junction solar cells accommodate the contacts for both polarities on the rear side of the solar cell. While efficient performance of this device structure strongly relies on a very high quality of front surface passivation, SunPower Corporation has already proven very high solar cell efficiencies of 22% and more in production¹ and also other leading solar cell manufacturers explore the benefits of using back-

junction solar cell device structures.² Generally, the current collection efficiency of back-junction solar cells increases with increasing area fraction of the minority charge carrier collecting p - n junction between emitter and absorber. On the other hand, this asymmetry is disadvantageous for the metal contacts as the metallisation of both polarities have to carry the same current. The minimisation of electrical series resistance and the cost-driven preference for thin layers of metal is a strong driving force towards metallisation designs that allocate similar area fractions for the metallisation of both polarities. Consequently, dielectric insulation layers may be used to meet both requirements: asymmetric base and emitter area fractions in the semiconductor and at the same time symmetric area fractions for the metallisation of base and emitter. Figure 1 shows a cell with dielectric insulation²: A reliable insulation layer allows using an overlap between e.g. the metallisation of the base with areas taken in by the emitter as shown in Figure 1.

* Correspondence to: Nils-P. Harder, Institute for Solar Energy Research Hameln GmbH (ISFH), D-31860 Emmerthal, Germany.

[†]E-mail: harder@isfh.de

[‡]Director of the Institute for Solar Energy Research Hameln GmbH (ISFH) and Professor of Physics at the Leibniz University Hannover.

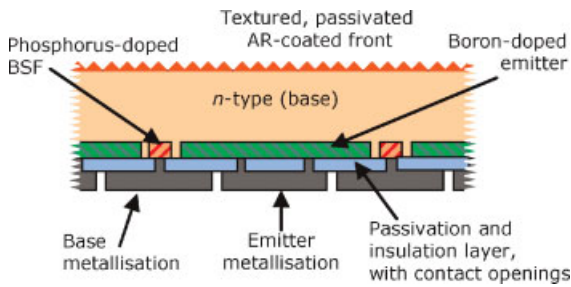


Figure 1. Cross sectional view of a back-junction solar cell with a large area fraction covered by the emitter, and similar area fractions allocated for base and emitter metallisation

In microelectronic applications thermal oxides have proven to fulfil such insulation purpose very efficiently when grown on polished wafers. However, as the silicon wafer material for commercial photovoltaic application has a rather rough surface and is not polished as in microelectronics, it is a challenging task to fabricate a reliable insulation layer by a thermal oxide.³ We therefore recently introduced the concept of the buried emitter solar cell (BESC)^{4,5} that does not rely on dielectric insulation. Figure 2 shows a schematic cross section of the BESC, which uses a p - n junction to shield the metallisation of the base from the large area emitter. This solar cell concept features large areas of overlap between heavy p -type and heavily n -type doped regions which is known to potentially give rise to junction shunting via trap assisted tunnelling.⁶ Such junction shunting would be highly detrimental for the fill factor of the solar cell and would lead to very low solar cell efficiencies.

It is therefore necessary that boron and phosphorus diffusion are well controlled and optimised in order to

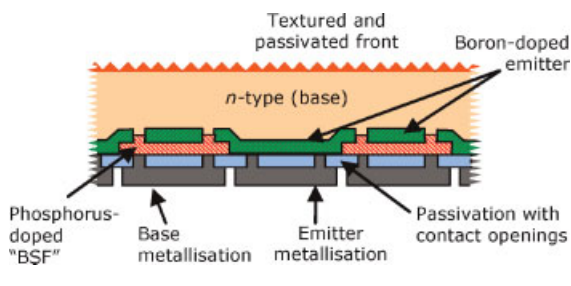


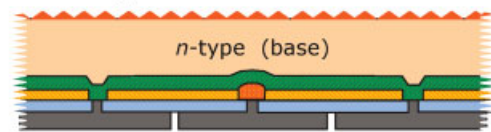
Figure 2. Cross-sectional view of a 'buried emitter' back-junction solar cell. The buried emitter solar cell exhibits a large area emitter, and the possibility of using similar area fractions for base and emitter metallisation without the need for any dielectric insulation. Note that the boron-doped emitter has only point-like openings. Thus, it is contiguous and covers virtually the full area

avoid such parasitic effects. However, once successfully implemented, the solar cell does not suffer from junction shunting and exhibits a reverse breakdown at relatively low voltages and the associated heat dissipation is distributed across the whole area of the cell. Consequently, localised hot spots can be avoided and solar modules made from BESC do not require installing separate bypass diodes. At present, our BESC development has reached solar cell efficiencies of 19.5% without any performance limitations due to shunting.⁵ In this paper, we investigate the current mechanisms and device performance with particular attention to the regions of n^+/p^+ overlap.

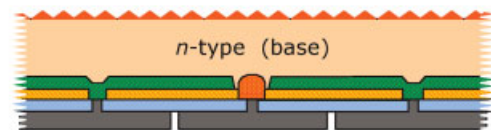
INVESTIGATED STRUCTURES AND SIMULATION MODEL

Figure 3. shows three variants of the BESC. All three structures have in common that virtually the entire rear side of the solar cell features phosphorus doped

A - Floating absorber



B - All contacted



C - Floating rear

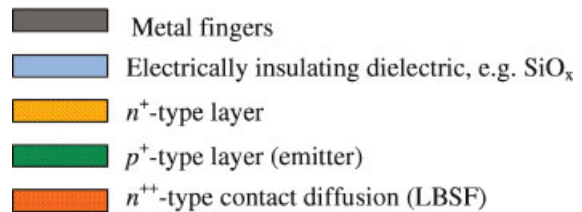
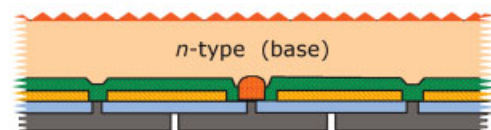


Figure 3. Cross-sectional view of three types of buried emitter back-junction solar cells: 'A-Floating absorber', 'B-All contacted' and 'C-Floating rear'

surfaces. These structures may therefore be considered as representing only that part of the BESC of Figure 2 that is covered by the base metallisation. Alternatively, the structures in Figure 3 may be considered as a generalisation of the BESC concept (shown in Figure 2), where now virtually the entire emitter is 'buried' under a layer of 'base-type' semiconductor. This is of particular interest for silicon solar cell with an *n*-type base with a *p*-type emitter: as opposed to boron-doped surfaces, phosphorus-doped surfaces are efficiently passivated by readily available thermal oxidation processes.^{5,7} The structures shown in Figure 3 therefore have the potential to generate high open-circuit voltages. However, this advantage comes at the price of having to face the challenge of implementing a reliable electrical insulation between base-type regions of the semiconductor and the metallisation of the emitter.

The 'A-Floating absorber' variant of the BESC is somewhat reminiscent of the thyristor structure solar cell, proposed and by Koschier and Wenham.⁸

For both, the thyristor structure solar cell and the floating absorber BESC, contacting of the majority charge carriers in the main absorber (electrons in *n*-type solar cells) occurs via transport through a layer in which these carriers are minority charge carriers. Once these carriers have traversed this layer (*p*-type emitter in the BESC in Figure 3A) they eventually reach a contacted surface layer where these carriers are majority charge carriers again.

The 'B-All contacted' BESC has perforations of the emitter and therefore the absorber and the base-type layer at the rear surface are in direct contact. Nevertheless both, base and emitter, are contiguous and thus all regions of the solar cell are directly contacted. As mentioned before, this 'B-All contacted' BESC can be regarded as a straight-forward generalisation of the BESC shown in Figure 2, or as representing only that part of the BESC of Figure 2 that is covered by the base-type surface layer.

The 'C-Floating rear' variant features a non-contiguous base-type (here: *n*-type) rear surface layer: at the rear side, only small area fractions of base-type are in direct contact with the main absorber volume. These regions are contacted by the base metallisation. However, the largest part of the rear side of the 'C-Floating rear' cell is covered by a floating junction to provide a similar passivation effect as achievable by a floating emitter.⁹

We investigate the performance of the three variants of the BESC by 1-dimensional device modelling

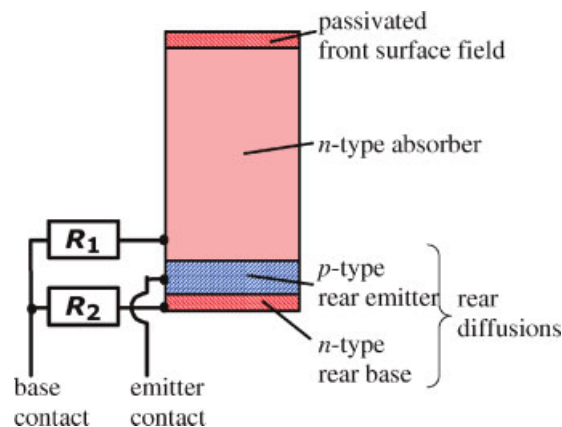


Figure 4. Schematic of the 1-dimensional PC1D model used for device simulation of the three generalised buried emitter solar cell concepts shown in Figure 3. Variant 'A-Floating absorber' is modelled by setting R_1 to very large resistance values and R_2 to zero. Variant 'B-All contacted' is realised by setting both resistances R_1 and R_2 to zero, while variant 'C-Floating rear' is represented by large resistance values for R_2 and zero for R_1 .

using PC1D.¹⁰ Figure 4 shows the structure of the PC1D model that we use for simulating the characteristics of the BESC. The minority charge carrier collecting *p-n* junction between emitter and absorber covers virtually the full area of the solar cell and therefore justifies simulating the minority charge carrier flow by a 1-dimensional PC1D model. The lateral current flows in BESC primarily occur in the form of majority charge carrier transport, which are neglected in our 1-dimensional treatment here.

Note that all three structures of Figure 3 are represented by the model shown in Figure 4 when choosing appropriate values for the resistances R_1 and R_2 : the 'A-Floating absorber' cell is modelled by setting R_1 to very large resistance values (e.g. $10^6 \Omega\text{cm}^2$) and R_2 to zero. The 'B-All contacted' cell is modelled when setting both resistances R_1 and R_2 to zero, while the 'C-Floating rear' cell is represented by assigning large resistance values (e.g. $10^6 \Omega\text{cm}^2$) to R_2 and zero resistance to R_1 .

Figure 5 shows the rear side doping profiles used for 1-dimensional numerical PC1D device simulations. The solid symbols are diffusion profiles as measured by electrochemical capacitance voltage (ECV) profiling at the rear side of the regions of diffusion overlap of an experimentally realised BESC.⁵ The ECV-measured boron doping profile corresponds to a sheet resistance of approximately 55 ohm/square and the phosphorus doping profile at the surface corresponds to

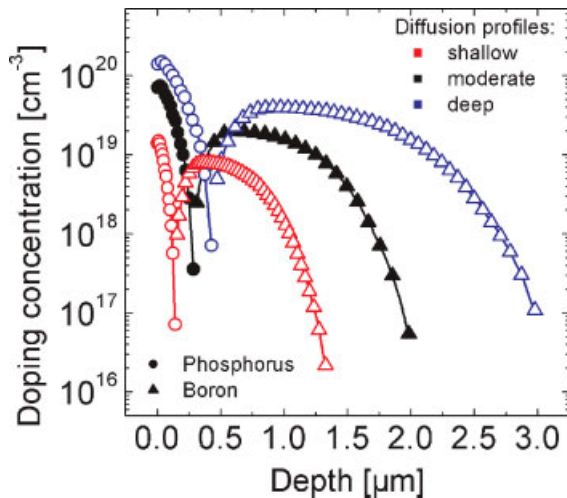


Figure 5. Solid symbols: doping profile of the surface region, where phosphorus diffusion has been performed into a previously boron diffused surface as measured by electrochemical capacitance voltage profiling (solid symbols). The open symbols represent modified doping profiles for investigating the influence of doping strength and depth by PC1D device simulations

a sheet resistance of about 90 ohm/square. The open symbols in Figure 5 are modified doping profiles that we use in our simulations in addition to the measured profile to also investigate different strengths and depths of the rear diffusions. We assign to each of the doping profiles a value of the surface recombination parameter S that depends on the donor surface concentration. Here we use the relation as determined by Cuevas *et al.*¹¹ Note that our one-dimensional simulation approach fully neglects the recombination contribution from the metal/semiconductor contacts and also neglect lateral current flows in the vicinity of the contacts. However, due to the small area fractions covered by these regions (in the range of a couple per cent) the associated effects can be regarded as small.

SIMULATIONS RESULTS AND DISCUSSION

Figure 6 provides an overview of the main simulation results obtained for all three solar cell structures shown in Figure 3, as modelled by the PC1D model sketched in Figure 4 and using a device thickness of 145 μm . The horizontal axis references the two resistors of the simulation model, R_1 and R_2 . As indicated by the uppermost horizontal axis in Figure 6, R_2 is held at $0 \Omega\text{cm}^2$ in the right part of each graph, while its value increases in the left part of each graph, while its value

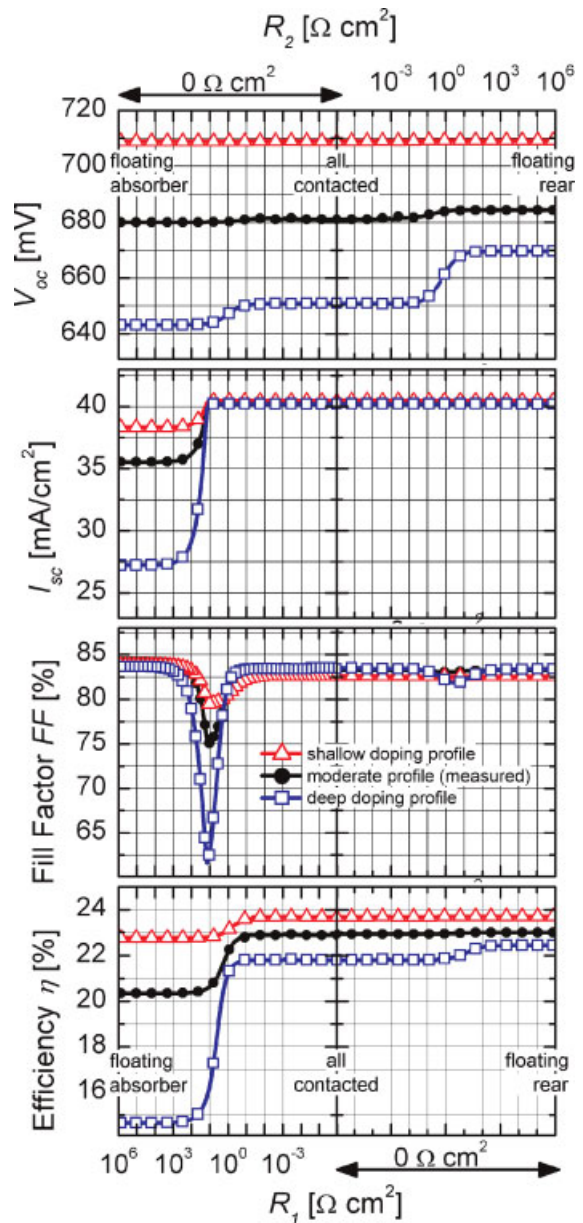


Figure 6. Performance of the model of Figure 4, as a function of resistance R_1 (lowermost axis) and R_2 (uppermost axis). Each curve corresponds to one of the p^+/n^+ doping profiles of Figure 5. The left of each graph ($R_1 = \text{large}$, $R_2 = 0$) represents the 'floating absorber' (Figure 3A), the centre ($R_1 = R_2 = 0$) represents the 'all contacted' case (Figure 3B) and the right ($R_1 = 0$, $R_2 = \text{large}$) represents 'floating rear' cells (Figure 3C)

increases in the right part of each graph (scale for R_2 increases from left to right). Conversely, R_1 is held at $0 \Omega\text{cm}^2$ in the right part of each graph, while its value increases in the left part of each graph as indicated by

the horizontal axis at the *bottom* of Figure 6 (scale for R_1 increases from right to left). As indicated in Figure 6, the ‘A-Floating absorber’ BESC is realised in its purest form at the left end of each graph (R_1 large, and $R_2 = 0 \Omega\text{cm}^2$). The centre of each graph represents the ‘B-All contacted’ case ($R_1 = R_2 = 0 \Omega\text{cm}^2$) and the right hand side of each graph corresponds to the ‘C-Floating rear’ BESC ($R_2 = 0 \Omega\text{cm}^2$ and R_2 large). There are three curves in each graph of Figure 6. Each of these three curves represent the simulation results obtained for one of the three n^+/p^+ double diffusion profiles of Figure 5.

Discussion of the open-circuit voltage

In accordance with general experience, the solar cell simulation that assumed the weakest (shallow) doping profiles, produces the highest calculated open-circuit voltages. More importantly, one can observe a clear hierarchy between the three concepts ‘‘C-Floating rear’’, ‘‘B-All contacted’’ and ‘‘A-Floating absorber’’. The highest voltages are achieved for the ‘‘C-Floating rear’’ case, whilst the ‘‘B-Floating absorber’’ produces the lowest voltages. At the same time it can be observed as well, that the open-circuit voltage differences between these three solar cell concepts become marginal in case of the shallow diffusion profiles. Taking the ‘‘C-Floating rear’’ case as the reference point, we shall now argue why the ‘‘B-All contacted’’ case produces lower voltages. The charge carrier generation rate at the rear is only marginal relative to the charge carrier generation in the bulk -and particularly compared to the generation close to the front surface of the solar cell. Consequently, virtually all excess charge carriers at the very rear of the solar cell have been generated elsewhere and are transported through the semiconductor to the rear.

The voltage of the solar cell equals the difference of the quasi-Fermi energies at base and the emitter contacts. However, in order to bias the floating junction between the emitter and the base layer on the rear side of the emitter, photogenerated charge carriers have to be transported from the n -type absorber region through the emitter to the floating base-type layer at the rear of the solar cell. That is, electrons have to diffuse as minority charge carriers through the p -type emitter towards the floating junction at the rear. Particularly in case of the heavy and deep doping profiles, the rear side of the solar cell is a relatively strong sink for charge carriers and therefore even under open-circuit conditions there is a permanent current flow of

electrons from the absorber through the emitter towards the floating junction at the rear. The bias level of the floating junction at the rear of the emitter can be well understood by considering the generalised expression for drift plus diffusion current

$$J_n = q\mu_n n \nabla E_{F,n} \quad (1)$$

and noting that the electron concentration n is very low within the rather heavily doped p -type emitter. J_n is the electron current, q the elemental charge, μ_n the electron mobility, n the electron concentration and $\nabla E_{F,n}$ the gradient of the quasi-Fermienergy of the electrons. The electron concentration n is very low within the heavily doped emitter. Thus, already relatively small electron currents J_n are associated with a strong gradient of the electron quasi-Fermilevel $\nabla E_{F,n}$ within the emitter, resulting in a considerable reduction of the electron quasi-Fermilevel at the rear junction. This effect is illustrated in Figure 7, showing the quasi-Fermilevel of electrons and holes of all three solar cell types under open-circuit conditions. It can

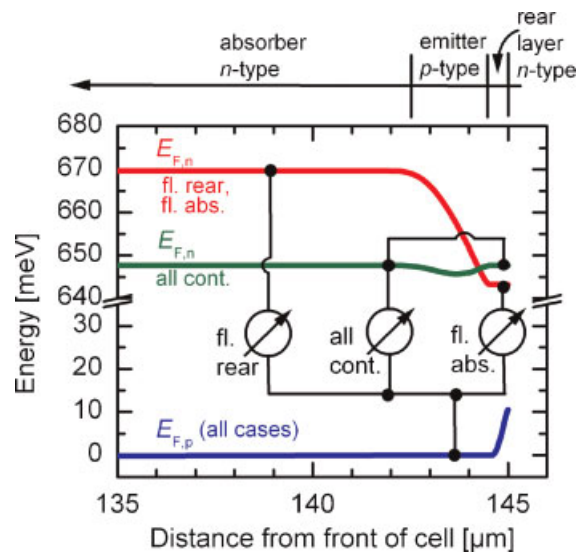


Figure 7. Electron and hole quasi-Fermi levels of the PC1D model (Figure 4) under open-circuit conditions, plotted for all three types of solar cells shown in Figure 3: ‘C-Floating rear’ (fl. rear), ‘B-All contacted’ (all cont.) and ‘A-Floating absorber’ (fl. abs.). The simulations assumed the deep n^+/p^+ diffusion profile shown in Figure 4. The contacting scheme of the three solar cell types is schematically indicated. Note that the quasi-Fermi level of the holes is very similar for all three types of solar cell. Furthermore, the electron quasi-Fermi levels of the ‘C-Floating rear’ and of the ‘floating absorber’ solar cell are virtually identical

clearly be seen that the energy difference between electron and hole quasi-Fermilevels is lower at the floating p - n junction at the rear of the emitter compared to the p - n junction between emitter and absorber. Therefore, the floating junction at the rear of the BESC operates at a lower “local voltage” than the externally measured open-circuit voltage of the “C-Floating rear” type cell. This effect is more pronounced for stronger doping and deeper emitters.

As opposed to the “C-Floating rear” case, in the “B-All contacted” BESC, the low resistance of R_1 and R_2 enforces the externally measured open-circuit voltage onto both, the junction at the rear and the junction between emitter and absorber, as visible in Figure 7. This biases the rear junction to a higher level and consequently causes increased total recombination within the device. As a result, the open-circuit voltage of the “B-All contacted” case is reduced in comparison to the “C-Floating rear” case.

The analysis of the voltage step in the left part of the open-circuit voltage in Figure 6 leads to very similar considerations. As indicated in Figure 7, under open-circuit conditions the quasi-Fermilevel curves of both electrons and holes are identical for the “C-Floating rear” and the “A-Floating absorber” solar cell structure. However, in case of the “A-Floating absorber” configuration contact is made to the lowly biased junction at the rear side of the emitter. Consequently, the externally measured voltage is lower compared to the other two configurations.

It is interesting to note that despite potentially considerable differences in open-circuit voltages between the “A-Floating absorber” and the “C-Floating rear” solar cell, the effective charge carrier lifetimes within the volume of these devices is the same for both solar cell concepts. Measurements of the effective lifetime of the charge carriers within the “A-Floating absorber” device and their interpretation as implied current-voltage characteristics¹² may lead to substantially higher open-circuit voltage predictions than the actually measured external open-circuit voltage. This discrepancy stems from the rather unfavourable way of contacting the base in case of the “A-Floating absorber” device, particularly for rather deep and heavily doped n^+ and p^+ layers at the rear of the solar cell.

Discussion of the short-circuit current density

The most prominent feature of the short-circuit current behaviour in Figure 6 is a drastic reduction of the short-

circuit current density for large values of the resistor R_1 , that is in case of the ‘A-Floating absorber’ concept. The value of the other resistor, R_2 , does not significantly influence the short circuit current density and thus the ‘B-All contacted’ and the ‘C-Floating rear’ BESC structure produce virtually identical short-circuit current densities. For these latter two concepts, the short-circuit current density is not very much influenced by the choice of the rear doping profiles. However, in case of the ‘A-Floating absorber’ concept the rear doping profiles have a remarkable effect on the short-circuit current density: the short-circuit current of the ‘A-Floating absorber’ solar cell reduces for deeper and heavier emitter doping.

To explain this behaviour we consider the electron current flow in the ‘A-Floating absorber’ configuration (R_1 very large and $R_2 = 0 \Omega$): in this case, the electrons (majority carriers within the n -type absorber) have to traverse the emitter region as minority charge carriers by diffusion before they eventually reach the base contact metallisation. Supporting large current densities by minorities in heavily-doped regions requires a large gradient of the respective quasi-Fermilevel as described by equation (1). This effect is further illustrated in Figure 8, where the energy band edges and electron and hole quasi-Fermilevels of a ‘A-Floating absorber’ BESC are shown under short circuit conditions.

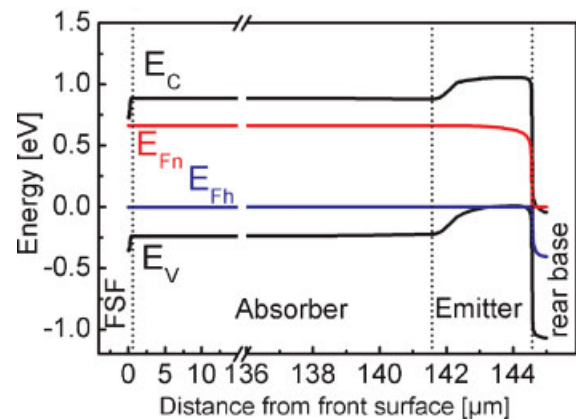


Figure 8. Energy band diagram of the one dimensional PC1D model for the ‘A-Floating absorber’ buried emitter solar cell as shown in Figure 4 (with R_1 very large, $R_2 = 0 \Omega \text{cm}^2$) under short circuit conditions. The front surface field, absorber, emitter and rear base regions are separated by dotted lines. Note that even under short-circuit conditions there is a high quasi-Fermilevel splitting at the absorber-emitter interface, which is characteristic for this cell structure variant ‘A-Floating absorber’

Note that the electron current flow through the emitter produces a very large energy difference between the two quasi-Fermilevels at the p - n junction between absorber end emitter despite external short-circuit conditions. The bias level of this p - n junction between emitter and absorber is comparable with open-circuit voltage bias levels. Consequently, there is a high level of recombination within the ‘floating absorber’, limiting the current collection efficiency drastically even under short-circuit condition.

Contacting the majority charge carriers directly at the absorber such as in the ‘B-All contacted’ or in the ‘C-Floating rear’ configuration of the BESC (Figure 3B and C) avoids the loss of free energy that results from transporting electrons across the p -type emitter. Consequently, there are only minor recombination losses for these latter two configurations under short-circuit conditions and the resulting short-circuit current densities are correspondingly high.

Discussion of the fill factor

The fill factor curves in Figure 6 shows two distinctive features in the form of reduced values for certain resistance values R_1 and R_2 . The first ‘fill factor dip’ occurs at the transition between the ‘A-Floating absorber’ configuration and the ‘B-All contacted’ configuration. The comparison with the short-circuit behaviour in Figure 6 indicates that this fill factor dip is associated with the change of magnitude of the solar cell current, as is illustrated in more detail in Figure 9.

The second fill factor dip in Figure 6 is much smaller and occurs at the transition between the ‘B-All contacted’ configuration ($R_1=0$, $R_2=0$) and the ‘C-Floating rear’ configuration ($R_1=0$, $R_2=large$). At this transition, there is hardly any change in short-circuit current visible but instead a rather pronounced change in open-circuit voltage can be observed.

Apart from the rather eye-catching fill factor dips in Figure 6, it is also striking that the ‘A-Floating absorber’ solar cell configuration produces very high fill factors at all: the inefficient electron transport through the p -type emitter in the ‘A-Floating absorber’ configuration limits current extraction to such an extent that even the short-circuit current density is reduced. On the other hand, the high fill factors of the ‘A-Floating absorber’ I - V curves do not seem to indicate any other transport related limitations. We shall therefore discuss the I - V curve of the ‘A-Floating absorber’ solar cell by developing an analytic description of this type of cell.

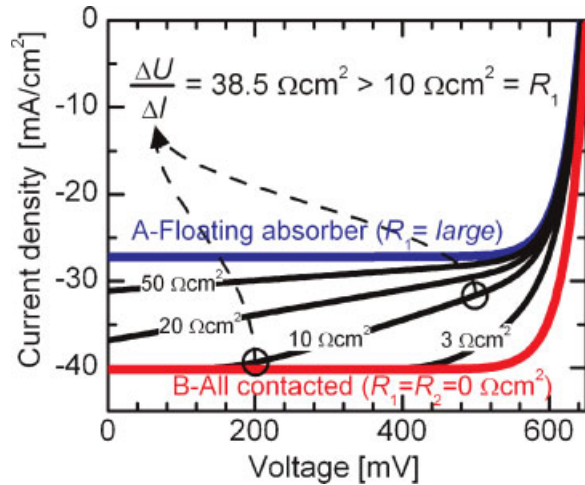


Figure 9. Simulated I - V curves under illumination, using the simulation model of Figure 4 and the deep doping profile of Figure 5. R_2 is held at $0 \Omega\text{cm}^2$, and is R_1 varied to explore the transition between the ‘A-Floating absorber’ (Figure 3A) and the ‘B-All contacted’ (Figure 3B) configuration. Note that the slope of the linear regions does not directly correspond to the magnitude of the resistor R_1

One may envisage the ‘A-Floating absorber’ type cell as a cell, where the majority carriers in the absorber are (directly) contacted via a resistor R_E , representing the non-ohmic resistance of the electron transport through the p -type emitter. We define an ‘internal voltage’ V_{int} at the p - n junction between emitter and absorber by

$$qV_{\text{int}} = E_{F,n,\text{absorber}} - E_{F,p,\text{emitter}} \quad (2)$$

where $E_{F,n,\text{absorber}}$ is the quasi-Fermienergy of the electrons in the absorber just outside the space-charge region of the junction, and $E_{F,p,\text{emitter}}$ is the quasi-Fermienergy of the holes in the emitter. At a given external voltage V_{ext} , the ‘A-Floating absorber’ cell produces a current output $J(V_{\text{ext}})$ and a voltage drop across the non-ohmic resistor R_E

$$V_{\text{int}} - V_{\text{ext}} = R_E \times J(V_{\text{ext}}) \quad (3)$$

With this equation defining R_E , we may now formally write the diode equation of the ‘A-Floating absorber’ solar cell as

$$J(V_{\text{ext}}) = J_0 \left(e^{q(V_{\text{ext}} + R_E \times J(V_{\text{ext}}))/kT} - 1 \right) - J_L \quad (4)$$

where J_L is the maximum extractable photo-generated current density within the absorber (i.e. at $V_{\text{int}}=0$), and J_0 is the saturation current density of the solar cell. The

solar cell absorber is now ‘directly’ contacted via R_E . This situation is similar to the ‘C-Floating rear’ configuration with the resistor $R_2 = \infty$ and $R_1 = R_E$ (see Fig. 4). We may therefore consider J_0 in equation (4) as being identical with the saturation current density of the ‘C-Floating rear’ solar cell configuration. This is also supported by Figure 7, showing identical quasi-Fermi-level distributions under open-circuit conditions for both the ‘A-Floating absorber’ and the ‘C-Floating rear’ configuration. Correspondingly, J_L in Equation (4) can be regarded as identical to the short-circuit current density of the ‘C-Floating rear’ solar cell configuration. For simplicity of the mathematical description we may further assume that the photo-generation of charge carriers within the rear emitter is negligible and that the doping profile of the p -type emitter is uniform. We can now readily calculate the electron distribution in the emitter by solving the well-known differential equation¹³

$$\frac{d^2 \Delta n}{dx^2} = \frac{\Delta n}{D_n \tau_n} \quad (5)$$

Where Δn is the excess electron concentration in the p -type emitter, D_n is the electron diffusion coefficient and τ_n is the lifetime of the electrons in the emitter. The solution of this differential equation has to fulfil the two boundary conditions

$$\begin{aligned} \Delta n(x=0) &= \frac{n_{i,\text{eff}}^2}{N_A} (e^{qV_{\text{ext}}/kT} - 1), \\ -qD_n \left. \frac{d\Delta n}{dx} \right|_{x=0} &= J(V_{\text{ext}}) - J_{0,\text{rB}} (e^{qV_{\text{ext}}/kT} - 1) \end{aligned} \quad (6)$$

where $n_{i,\text{eff}}^2$ is the effective intrinsic carrier concentration that is subject to band-gap narrowing,¹⁴ N_A is the dopant density in the emitter, $J_{0,\text{rB}}$ is the saturation current density of the base-type (n -type) layer at the rear of the solar cell, and $x=0$ denotes the position of the edge of the space-charge region of the p - n junction between the emitter and the rear base-type layer. According to the chosen sign-convention, an electron current J_n from the emitter towards the rear base-type layer (i.e. in direction of negative values of the variable x) is counted as negative. The recombination current $J_{0,\text{rB}} (e^{qV_{\text{ext}}/kT} - 1)$ has a positive sign as it is a current flowing from the contact at the rear base-type layer into the cell towards the emitter. For positive values of V_{ext} we therefore have $|J(V_{\text{ext}}) - J_{0,\text{rB}} (e^{qV_{\text{ext}}/kT} - 1)| > |J(V_{\text{ext}})|$. The position $x=W$ shall correspond to the other side of the emitter, that is the edge of the space

charge region of the p - n junction between the absorber and the emitter. The electron concentration at this position defines the internal voltage V_{int}

$$V_{\text{int}} = \frac{kT}{q} \ln \left(\frac{N_{\text{dop}} \Delta n(W)}{n_i^2} + 1 \right) \quad (7)$$

Combining the solution $\Delta n(x)$ of the differential equation (5) with (3) and (7) yields an expression for the non-ohmic resistance R_E

$$\begin{aligned} R_E(V_{\text{ext}}) &= \frac{V_{\text{int}} - V_{\text{ext}}}{J(V_{\text{ext}})} = \frac{1}{J(V_{\text{ext}})} \\ &\bullet \left\{ \frac{kT}{q} \ln \left[\frac{\left(e^{\frac{qV_{\text{ext}}}{kT}} - 1 \right) \cosh \left[WN_A \sqrt{\frac{C_p}{D_n}} \right]}{J(V_{\text{ext}}) - J_{0,\text{rB}} \left(e^{\frac{qV_{\text{ext}}}{kT}} - 1 \right) \sinh \left[WN_A \sqrt{\frac{C_p}{D_n}} \right]} \right] - V_{\text{ext}} \right\} \end{aligned} \quad (8)$$

In equation (8) we have assumed that the electron lifetime τ_n is dominated by Auger recombination, that is $\tau_n = (C_p N_A^2)^{-1}$, where C_p is the Auger coefficient for the two-hole-one-electron (ppn) Auger recombination process. Inserting equation (8) into equation (4) yields an expression that resembles a simple diode equation

$$\begin{aligned} J(V_{\text{ext}}) &= J_0 \frac{\left(\frac{qn_{i,\text{eff}}^2 \sqrt{C_p D_n}}{\tanh \left[WN_A \sqrt{C_p / D_n} \right]} + J_{0,\text{rB}} \right)}{\left(\frac{qn_{i,\text{eff}}^2 \sqrt{C_p D_n}}{\sinh \left[WN_A \sqrt{C_p / D_n} \right]} + J_0 \right)} \\ &\times \left(e^{\frac{qV_{\text{ext}}}{kT}} - 1 \right) - \frac{J_L}{\left(1 + \frac{J_0 \sinh \left[WN_A \sqrt{C_p / D_n} \right]}{qn_{i,\text{eff}}^2 \sqrt{C_p D_n}} \right)} \end{aligned} \quad (9)$$

We can see from equation (9) that the voltage dependence of the non-ohmic series resistance R_E is of such a kind that the shape of the ‘A-Floating absorber’ I - V curve has the appearance as if there was no series resistance at all. The resistance value of R_E decreases for increasing external voltages V_{ext} as higher voltages increase the electron concentration in the p -type emitter exponentially. Consequently, equation (9) provides an explanation, why the ‘A-Floating absorber’ configuration produces I - V curves with very high fill factors despite a very severe limitation of the electron current flow through the p -type emitter. The prefactor of the exponential term in equation (9) shall be called ‘apparent saturation current density’ $J_{0,\text{A}}$. $J_{0,\text{A}}$ is the product of the original saturation J_0 and a second factor that also depends on J_0 . Surprisingly, $J_{0,\text{A}}$

can become smaller than J_0 , particularly for very large values of J_0 . However, in agreement with expectation, in case of large saturation current densities J_0 , equation 9 still *does not* predict higher open-circuit voltages for the ‘A-Floating absorber’ compared to the ‘C-Floating rear’ cell, because larger J_0 values at the same time over-proportionally decrease the modified short-circuit current density in equation (9): the last term in equation (9) resembles the short circuit current density of the ‘A-Floating absorber’ cell, which decreases for increasing J_0 . This effect has also been found for the numerical PC1D simulations shown in Figure 6. In particular we can see from equation (9) that the modified short-circuit current density of the ‘A-Floating absorber’ cell is always smaller than the short-circuit current density J_L of the ‘C-Floating rear’ cell. Again, this analytical finding agrees well with the I - V curves simulated by PC1D in Figure 9.

We shall now discuss the fill factor dip in the transition between the ‘A-Floating absorber’ and the ‘B-All contacted’ configuration, as shown in the left part of Figure 6. The transition from the ‘A-Floating absorber’ configuration to the ‘B-All contacted’ cell is made by lowering the resistance value for R_1 , which provides an additional transport path for extracting the electrons out of the cell. Figure 9 illustrates the shape of the I - V curves upon changing the resistance value R_1 . These curves seem to suggest that the higher current of the ‘B-All contacted’ BESC *could* be understood as a combination of a ‘baseline’ of current transported through the emitter plus an additional current through the resistor R_1 . However, the partially linear slope of the I - V curves in Figure 9 does not directly relate to the series resistance of R_1 as indicated in the same Figure. Instead, the current paths and injection conditions within the cell are changed completely by lowering the resistance of R_1 . This is illustrated in Figure 10, showing the magnitudes of the electron currents flowing through the p -type emitter (R_E) and through R_1 for a range of values of R_1 and an external voltage $V_{\text{ext}} = 500$ mV.

Low resistance values R_1 level out the difference between the internal voltage V_{int} , defined in equation (2), and the external voltage V_{ext} . Consequently, low values of R_1 prevent the excessive splitting of the electron and hole quasi-Fermi levels that has been identified in Figure 8 for being responsible for the inefficient current collection. The key criterion for the magnitude of R_1 to achieve the increase of current is that R_1 has to be significantly smaller than R_E . However, R_E is strongly dependent on the external

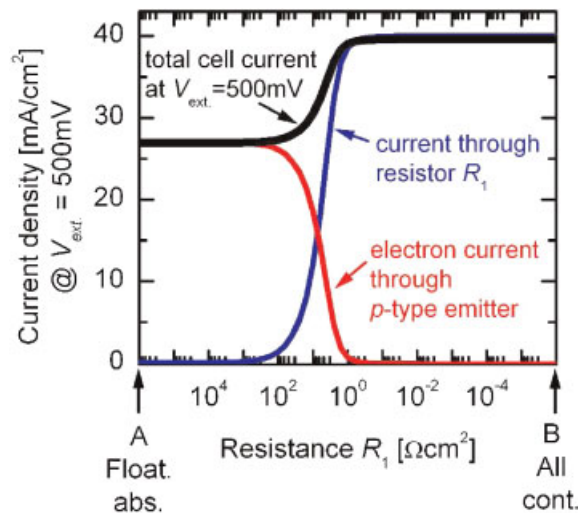


Figure 10. Simulated total cell output current and the electron current flows through the p -type emitter and through the resistor R_1 . The external voltage was held at 500 mV. This simulation assumed the deep p^+/n^+ doping profile shown in Figure 4

voltage V_{ext} and therefore small and medium values of R_1 (e.g. $10 \Omega\text{cm}^2$) are only capable of increasing the current in the vicinity of short-circuit conditions, see Figure 9. In this situation the current density is hardly changed in the vicinity of the maximum power point and consequently the fill factor drops to very low values for medium sized resistances R_1 . Further lowering the resistance R_1 down to values below $1 \Omega\text{cm}^2$ eventually increases the current at the maximum power point significantly and produces high fill factors again.

Despite a very different solar cell concept, this fill factor effect of the back-junction BESC is reminiscent of effects observable for emitter-wrap-through solar cells.^{15,16} It is further noted that despite the absence of any junction shunting the shape of the I - V curves in Figure 9 nevertheless do suggest the presence of junction shunting for small and intermediate resistance values of R_1 (e.g. $20 \Omega\text{cm}^2$) and may lead to an erroneous assessments of the loss mechanisms in experimentally prepared devices.

The second fill factor dip visible in the right hand side of Figure 6 is much smaller and lies in the transition region between the ‘B-All contacted’ configuration ($R_1 = 0$, $R_2 = 0$) and the ‘C-Floating rear’ configuration ($R_1 = 0$, $R_2 = \text{large}$). This second fill factor effect is only accompanied by a change in open-circuit voltage while there is no significant effect on the short-circuit current. The illustration of this

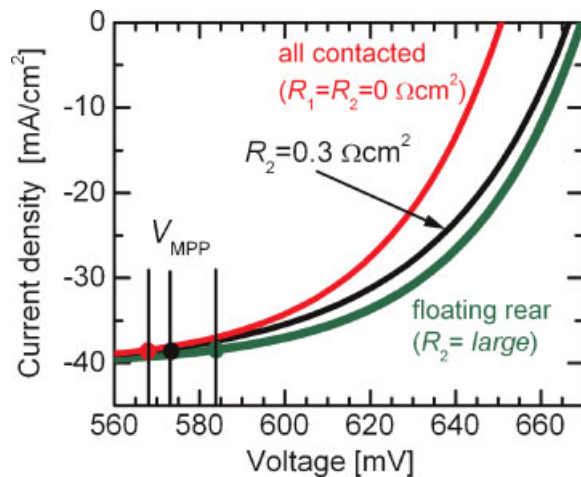


Figure 11. Simulated I - V curves under illumination, using the simulation model of Figure 4 and the deep doping profile of Figure 5. R_1 is held at $0 \Omega\text{cm}^2$. Three values for R_2 are used to explore the transition between the 'all contacted' case (Figure 3B) and the 'floating rear' (Figure 3C) configuration

second fill factor effect in Figure 11 therefore focuses onto the region of the I - V curve between maximum power point and open-circuit voltage. As indicated in Figure 11, for intermediate resistance values of R_2 the increase of the maximum power voltage is not proportional to the increase of the open-circuit voltage. For $R_2 = 0.3 \Omega\text{cm}^2$, the open-circuit voltage is already close to the 'C-Floating rear' case, but the maximum power point voltage is still closer to the 'B-All contacted' case. We therefore find a reduced fill factor in Figure 6 for $R_2 = 0.3 \Omega\text{cm}^2$. As this effect is coupled to changes of the open-circuit voltages, it is plausible that the magnitude of the fill factor effect scales with the magnitude of the open-circuit voltage effect discussed before (uppermost graph in Figure 6) and thus hardly affects the cell structures with rather weak doping profiles.

Discussion of the efficiency

The efficiencies of the three different BESC structures closely resemble the behaviour of the short-circuit current and the open-circuit voltage diagrams. The 'C-Floating rear' case gives the highest efficiencies and reaches 23.7% in our calculations for shallow doping profiles. However, in case of shallow doping profiles there is no significant difference in performance between the 'C-Floating rear' and 'B-All contacted' configuration. The simulations that used the experimentally realised doping profiles also produced only

minor differences in efficiency between the 'C-Floating rear' (23.0%) and the 'all contacted' (22.9%) case. However, heavy doping (deep n^+/p^+ doping profile in Figure 5) and the associated recombination at the rear of the solar cell produce a difference of 0.5% (absolute) between having floating base regions or contacted base regions at the rear side of the emitter. Compared to the similar performances of the 'C-Floating rear' and the 'B-All contacted' BESC, the 'A-Floating absorber' configuration exhibits significant reductions of the solar cell efficiency and reacts with pronounced voltage and current losses to heavier doping and deeper emitter layers. In terms of performance, the 'A-Floating absorber' does not seem to offer any advantages. However, from a technological point of view the advantage of this structure is that it does not require structuring the emitter layer.

All of the BESC structures shown in Figure 3 have in common that virtually all surface areas of these solar cells are phosphorus-doped despite featuring an almost full-area p -type (buried) emitter layer. The phosphorus-doped silicon surfaces can be efficiently passivated by standard thermal oxidation.¹¹ Therefore the BESC has the potential to reach very high solar cell efficiencies, as is reflected by the results of our simulations.

CONCLUSIONS

We have generalised the novel BESC concept and proposed three different device structures where a thermally oxidised n -type surface layer can be used for efficient surface passivation of p -type emitters. We have investigated the performance of the proposed three BESC structures by 1-dimensional device modelling, using the experimentally determined surface recombination parameters for oxidised n -type surfaces.¹¹ We have developed an analytical description of the unconventionally contacted 'A-Floating absorber' BESC variant and have been able to explain the open-circuit voltages, short-circuit current densities and fill factors of the three novel BESC devices. In particular, we show that the p -type emitter surface passivation is best achieved by a floating junction with an n -type layer on the emitter surface ('C-Floating rear' configuration). At the same time we find that a non-floating n -type surface layer that is in direct electrical contact with the n -type absorber ('B-All contacted' configuration) can provide almost the same quality of surface passivation if the doping profiles are not too heavy.

REFERENCES

- De Ceuster DM, Cousins P, Rose D, Vicente D, Tipones P, Mulligan W. Low Cost, High Volume Production of >22% Efficiency Silicon Solar Cells. *22nd European Photovoltaics Specialists Conference*, Milan 2007; 816–819.
- Huljic DM, Zerres T, Mohr A, v. Maydell K, Petter K, Müller JW, Feist H, Harder N-P, Engelhart P, Brendemühl T, Grischke R, Meyer R, Brendel R, Granek F, Grohe A, Hermle M, Schulz O, Glunz SW. Development of a 21% Back-Contact Monocrystalline Silicon Solar Cell for Large-Scale Production. *21st European Photovoltaic Specialists Conference (2006)*, Dresden, 2006; 765–768.
- Knoll D, Grabolla T, Bugiel E. Influence of mechanical stress on thermal oxidation phenomena of silicon. *Crystral Research and Technology* 1987; **22**: 713–722.
- Harder N-P. ISFH, patent pending. German patent application 10.2008.030.880.3-33.
- Harder N-P, Mertens V, Brendel R. Buried emitter solar cell structures: decoupling of metallization geometry and carrier collection geometry of back contacted solar cells. *Physica Status Solidi - Rapid Research Letters* 2008; **2**: 148–150. DOI: 10.1002/pssr.200802113
- Hurx GAM, Klaassen DBM, Knuvers MPG. A new recombination model for device simulation including tunnelling. *IEEE Transactions on Electron Devices* 1992; **ED-39**: 331–338.
- Benick J, Schultz-Wittmann O, Schön J, Glunz SW. Surface passivation schemes for high-efficiency n-type silicon solar cells. *Physica Status Solidi - Rapid Research Letters* 2008. **1–3**: DOI: 10.1002/pssr.200802124
- Koschier LM, Wenham SR. Improved open circuit voltage using metal mediated epitaxial growth in thyristor structure solar cells. *Progress in Photovoltaics* 2000; **8**: 489–501.
- Glunz SW, Biro D, Rein S, Warta W. Field-effect passivation of the SiO₂-Si interface. *Journal of Applied Physics* 1999; **86**: 683–691.
- Clugston D, Basore PA. PC1D Version 5: 32-Bit solar cell modeling on personal computers. *Proceedings of the 26th IEEE*, Anaheim California 1997; 207–210.
- Cuevas A, Basore PA, Dubois C. Surface recombination velocity of highly doped n-type silicon. *Journal of Applied Physics* 1996; **80**: 3370–3375.
- Sinton RA, Cuevas A, Contactless determination of current-voltage characteristics and minority-carrier lifetimes in semiconductors from quasi-steady-state photoconductance data. *Applied Physics Letters* 1996; **69**: 2510–2512.
- Green MA. Solar cells. *Operating Principles, Technology and System Applications*. Prentice-Hall, Inc.: Englewood Cliffs, N.J., 1982; 07632.
- Altermatt PP, Schenk AS, Geelhaar F, Heiser G. Reassessment of the intrinsic carrier density in crystalline silicon in view of band-gap narrowing. *Journal of Applied Physics* 2003; **93**: 1598–1604.
- Dicker J, Solter J, Schumacher JO, Glunz SW, Warta W. Analysis of rear contacted solar cell structures for cost-effective processes and materials, *28th IEEE Photovoltaics Specialists Conference* 2000; 387–390.
- Ulzhöfer C, Hermann S, Harder N-P, Altermatt PP, Brendel R. The origin of reduced fill factors of emitter-wrap-through-solar cells, physica status solidi (RRL). *Physica Status Solidi - Rapid Research Letters* 2008; **2**: 251–253. DOI: 10.1002/pssr.200802115